Design of a Spiral Coil for High-frequency Wireless Power Transfer Systems using Machine Learning

Minki Kim, Minoh Jeong, Student Member, IEEE, Martina Cardone, Jungwon Choi, Member, IEEE .

Abstract—This paper presents a novel design method based on machine learning (ML) for a spiral coil in a wireless power transfer (WPT) system operating at high frequencies. While a MHz frequency operation provides high power density for battery-powered applications, optimizing the spiral coil design becomes challenging due to the complex electromagnetic analysis, such as skin and proximity effects. Even though a threedimensional (3D) electromagnetic simulator provides a practical analysis of different coil structures, it cannot quickly optimize the coil design due to its computing time. Therefore, an MLbased method is first proposed to estimate the Q factor of a spiral coil, a critical parameter to determine the efficiency of a WPT system. Towards this end, a feed-forward neural network is trained using around $20 \cdot 10^3$ data samples collected by using a 3D quasi-static electromagnetic field simulator. It is shown that this method is effective; that is, it ensures an accuracy of up to 96%. Then, a spiral coil design method leveraging the designed ML-based Q factor estimation is proposed. This method offers high performance (the intersection over union metric takes values up to 70%) and significant computation time savings (at least five orders of magnitude), compared to commonly adopted software simulators. Finally, the effectiveness of the proposed method is verified by the actual fabrication of several spiral coils.

Index Terms—Spiral Coil Design, Wireless Power Transfer, Machine Learning.

I. INTRODUCTION

B ATTERY-powered vehicles, such as drones, robots, and automated guided vehicles, have attracted a lot of interest in moving toward electrification [1]–[3]. Whenever the battery power is sufficient, these vehicles act fast and widely, while carrying a heavy load and working repeatedly and tirelessly to perform a significant amount of labor. Therefore, these vehicles require convenient and flexible charging ways due to their scheduled and diligent workloads. A charging method using wireless power transfer (WPT) systems has the potential to increase productivity without any plug-in connections. In WPT systems, the power transmits through magnetic couplings between the charging stations and the batteries, without any cables or wires [4], [5]. Among the system components, the coupling coils are crucial to obtain a high efficiency in WPT systems and hence, it is paramount to extract their electrical characteristics. The lumped elements, such as the resistance R and the inductance L, are used to model the electrical properties of the coil. These elements also determine the

The authors are with the Electrical and Computer Engineering, University of Minnesota, Minneapolis, MN 55455 USA (e-mail: kim00756@umn.edu; jeong316@umn.edu; mcardone@umn.edu; jwchoi@umn.edu).

Portions of this work have been presented at the 2022 IEEE 23rd Workshop on Control and Modeling for Power Electronics (COMPEL) and at the 2023 IEEE Applied Power Electronics Conference and Exposition (APEC) [14], [15]

quality Q factor, which is the ratio between the reactance and the resistance in the circuit. A WPT system requires the coil to have a high Q factor by generating a low resistance. However, the mathematical model for R at MHz frequencies is complex due to the proximity, skin effect, and other hidden losses.

In addition to the importance of R of the coils, in WPT systems it is also necessary to consider the parasitic stray capacitance C_p of the spiral coils at MHz frequencies [6], [7]. In reality, the stray capacitance and inductance form a parasitic parallel resonance. When the operating frequency and the parasitic resonance frequency are close to each other, this parasitic capacitance can significantly decrease the performance of series resonant-based WPT systems at a high-frequency of operation [8]. Ignoring the stray capacitance can therefore cause unintended behavior in the coupling coefficient, or load variance of a series resonant-based compensation network (e.g. Series-Series, Series-Parallel, and LCC compensation network) [9], [10]. Thus, it is important to consider the parasitic stray capacitance and minimize its negative effects. The stray capacitance of a spiral coil is determined by several factors such as the diameter of each turn, the total number of turns, the pitch size, and the conductor permittivity. However, it is difficult to accurately calculate the self-capacitance due to the nonlinear adjacent winding capacitance, which depends on the structure of the coil [6]-[8].

In order to address the aforementioned issues, there are several software simulators based on numerical analyses for optimizing a coil design. Three-dimensional (3D) finite element method (FEM) solvers, such as Ansys-HFSS and COMSOL, are the most representative simulators for calculating the electrical characteristics. Also, a 3D quasi-static electromagnetic field simulator, such as Ansys-Q3D, can be used to extract directly the values of R, L, and C_p [11], [12]. However, these conventional methods are time-consuming and cannot provide insights into how to design and optimize the coil for a specific application. To address this issue, it is necessary to have a design method that is capable of quickly finding an optimal design when some parameters are given.

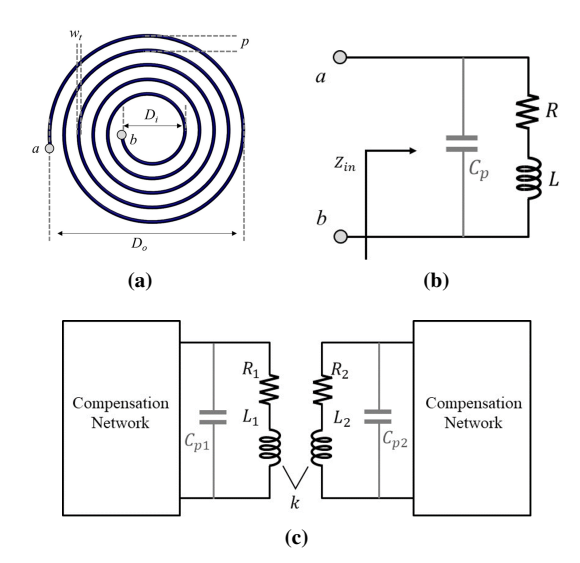
In this paper, we propose a machine learning (ML) method for high-frequency spiral coil design in WPT systems. High-frequency WPT systems have the potential to provide a compact and agile charging solution thanks to their reduced size and weight of their components. The practical applications of our research extend to battery-powered devices, including drones, robots, and automated guided vehicles. While we mainly focus on high-frequency (>1 MHz) coil designs in this paper, our methodology is applicable to coil designs in low-frequency operation. The contributions and the outline of

the paper are as follows:

- In Section II, we formally define the design parameters and electrical components of a spiral coil, as well as the Q factor, which is a critical parameter to determine the efficiency of a WPT system.
- In Section III, we propose an ML-based method to estimate the Q factor of a spiral coil. Specifically, we first build a dataset using the Ansys-Q3D simulator and then leverage it to train a feed-forward neural network (FNN) that outputs an estimate of the Q factor of the spiral coil under consideration. Our numerical evaluations showcase that the proposed ML-based Q factor estimation performs well (the average error rate is below 10%) even when only 10% of the data samples are used for training.
- In Section IV, we propose a spiral coil design method that leverages our ML-based Q factor estimation proposed in Section III. In particular, given the values of some spiral coil design parameters, namely the outer diameter Do and the wire thickness wt, the method estimates the remaining design parameters, namely the pitch size p, the frequency of operation fs and the number of turns N, that result in the highest Q factor of the coil. We assess the performance of the proposed method by using the intersection over union (IoU) [13] as a metric. Our results show the effectiveness of the proposed method both in terms of performance (IoU of 70%) and computation time (five orders of magnitude faster than Ansys-Q3D).
- In Section V, we present experimental results of the proposed coil design method of Section IV. We fabricate and test several spiral coils (which differ in their values of p, f_s, and N) and verify the effectiveness and computation efficiency of the proposed optimization method.
- In Section VI, we conclude the paper.

We build on our previous works [14] and [15]. However, this paper has the following key distinctive features from [14] and [15]:

- Searching parameters: In [14], the proposed method required three input parameters (namely, D_o , f_s , and w_t) to generate two output parameters (namely, p and N). This paper extends this setting: the method operates with just two input parameters (namely, D_o and w_t) and produces three output parameters (namely, f_s , p, and N). This extension of the method increases the dimension of the search space from two parameters to three parameters, showcasing that the proposed method is indeed versatile to different coil design scenarios.
- Methodology for top-k% region: In [15], we used the Clough-Tocher interpolation method to find the so-called top-k% region (see Section IV). Differently, here we use a machine learning approach. This not only simplifies the computational process, but it also offers a more intuitive (and potentially accurate) design.
- Experimental validation: This paper includes AC-to-AC WPT experiments to validate the effectiveness of the proposed method in terms of conversion efficiency. These experimental results are additional contributions which were not presented in [14] and [15].



2

Fig. 1: Structure of a spiral coil: (a) design parameters; (b) lumped elements model; and (c) WPT system structure.

II. SPIRAL COIL DESIGN

The geometry of a circular spiral coil consists of the outer diameter D_o , inner diameter D_i , number of turns N, pitch size p, and wire thickness w_t of the coil, as illustrated in Fig. 1a. These parameters are tied together by the following relationship,

$$D_o = D_i + 2N(w_t + p). (1)$$

The equivalent circuit of the spiral coil, shown in Fig. 1b, consists of the lumped elements of the spiral coil, namely the resistance R, the inductance L, and the capacitor C_p . The geometry parameters of the spiral coil and the values of R, L, C_p are approximately represented with the following simplified equation [7], [16],

$$R = R_{DC} \frac{w_t}{4\delta}, \ R_{DC} = \frac{l}{\sigma \pi (w_t/2)^2}, \ \delta = \frac{1}{\sqrt{\pi f_s \sigma \mu_o}}, \quad (2)$$

$$L = \frac{39.37N^2(D_o - N(w_t + p))^2}{16D_o + 28N(w_t + p)} [\mu H],$$
 (3)

$$C_p = 0.035D_o + 0.06 [pF],$$
 (4)

where R_{DC} is the DC resistance, l is the wire length, δ is the skin-depth, σ is the conductivity of the conductor, and μ_0 is the permeability of the free space. Based on the equivalent circuit, the input impedance Z_{in} of a spiral coil between nodes a and b (see Fig. 1b) is computed as,

$$Z_{in} = R_{eq} + jwL_{eq} = \frac{1}{jwC_p} ||(R + jwL)|$$

$$= \frac{R}{1 - 2C_pLw^2 + R^2C_p^2w^2 + L^2C_p^2w^4}$$

$$+ j\frac{wL - wC_pR^2 - C_pL^2w^3}{1 - 2C_pLw^2 + R^2C_p^2w^2 + L^2C_p^2w^4},$$
(5)

where w is the angular frequency.

The Q factor is the ratio between the reactance X_{eq} and the resistance R_{eq} of the input impedance, which also means that the Q factor measures the ratio between the stored energy and

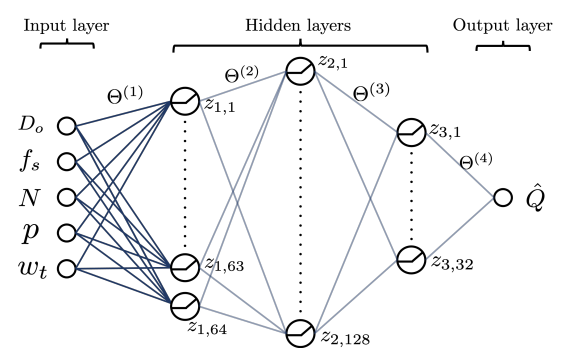


Fig. 2: FNN with three hidden layers and ReLU activation function.

the dissipated energy in the coil [17]. It is calculated by using the impedance of the spiral coil as follows,

$$Q = \frac{wL_{eq}}{R_{eq}} = \frac{X_{eq}}{R_{eq}} = \frac{w(L - C_pR^2 - C_pL^2w^2)}{R}.$$
 (6)

Then, the calculated Q factors of the coupling coils are used to find the efficiency of the WPT system. Fig. 1c shows a two-coil WPT system when the designed coils are used for the transmitter and receiver. When we consider the series-series compensation network, the maximum conversion efficiency of the WPT system is denoted as η_{max} and expressed as,

$$\eta_{max} = \frac{k^2 Q_1 Q_2}{\left(1 + \sqrt{1 + k^2 Q_1 Q_2}\right)^2},\tag{7}$$

where Q_1 and Q_2 are the quality factors of L_1 and L_2 , respectively, and k is the coupling coefficient between the two coils [18]. To guarantee high efficiency of the WPT system, it is necessary to find a high Q factor among the various designs of the spiral coils considering the application environments.

To estimate the Q factor, the lumped elements need to be calculated either by leveraging approximating expressions (2)-(4) or via simulations by 3D FEM solvers [11], [12]. Importantly, the resistance R should reflect all of the losses in the coil, and its value is complicated to estimate at MHz frequencies due to the proximity and skin-depth effects. Also, the parasitic stray capacitor must be considered since it induces parasitic self-resonance in the coil. In this work, since the approximating expressions cannot capture all of the parasitic effects, we utilize the Ansys-Q3D simulator to extract the values of R, L, and C_p . However, it took $2 \sim 4$ hours to simulate for 50 designs ($2 \sim 5$ minutes/design) using Ansys-Q3D. The computation time for the simulation is influenced by the coil structure and the frequency of the analysis.

III. QUALITY FACTOR CHARACTERIZATION USING MACHINE LEARNING

A. Prediction Using Deep Learning

ML [19] methods are widely used for approximating a large class of functions provided that there exists a dataset that properly represents the input and output of the function. Moreover, deep neural network (DNN) [20] models perform unprecedented achievements for various tasks, such as computer vision and natural language processing tasks. A basic

DNN consists of a number of layers, in which we distinguish an input layer, an output layer, and hidden layers. Each hidden layer has a number of neurons that perform a weighted sum on their incoming values, which is then followed by a non-linear activation function. Since the activation function is non-linear, the capacity of a DNN model is large enough to approximate any arbitrary function [21], [22].

In our setting, the estimation of the Q factor in (6) can be considered as a regression problem since the Q factor is a continuous value. A suitably designed DNN can then be leveraged to estimate the Q factor by approximating the true function between (D_o, f_s, N, p, w_t) and Q using the available dataset¹. To this end, we adopt an FNN [19], in which only fully-connected layers exist, i.e., all neurons in a layer are connected to every neuron in the next layer. Fig. 2 illustrates a simple FNN model designed with five input parameters, one output parameter, and three hidden layers. Each neuron in the hidden and output layers performs a weighted sum of all its incoming values. Then, at every neuron, a non-linear activation function is applied on the result of the sum and this is the output of the neuron. This operation is iteratively performed in every layer until the result arrives at the output layer.

With reference to Fig. 2, we denote by $z_{\ell,i}$, $\ell \in \{0, 1, 2, 3, 4\}$ the output of the *i*th neuron in the ℓ th layer, and the operation at every neuron is formally expressed as,

$$z_{\ell,i} = \sigma\left(\left\langle \Theta_i^{(\ell)}, u_\ell \right\rangle + b_i^{(\ell)}\right),$$
 (8)

where: (i) $\sigma(\cdot)$ is a non-linear activation function; (ii) $\langle \cdot, \cdot \rangle$ denotes the inner product; (iii) $\Theta_i^{(\ell)}$ is the weight vector for the ith neuron in the ℓ th layer, and $\Theta^{(\ell)}$ is obtained by stacking together all the $\Theta_i^{(\ell)}$'s; (iv) u_ℓ is the input vector of the ℓ th layer; and (v) $b_i^{(\ell)}$ is the bias term, which is a constant that helps the model to best fit the given data. Here, the $z_{0,i}$'s (i.e., the input parameters) are the parameters of the problem of interest, i.e., D_o, f_s, N, p , and w_t . In particular, we set the number of neurons in each hidden layer to 64,128, and 32, respectively, and we consider the rectified linear unit (ReLU) activation function $\sigma(x) = \max\{0, x\}$. By calculating $z_{\ell,i}$ for all i's, the output vector of the ℓ th layer (i.e., z_ℓ) is obtained by stacking together the $z_{\ell,i}$'s and it can be used as the input vector of the $(\ell+1)$ th layer if $\ell \in \{1,2,3\}$ (i.e., $u_{\ell+1} = z_\ell$), or as the output of the FNN if $\ell=4$. The estimated output value, denoted as \hat{Q} , can then be expressed as $\hat{Q} = \sum_{k=1}^{32} \Theta_{1,k}^{(4)} z_{3,k} + b_1^{(4)}$, where $\Theta_{1,k}^{(4)}$ is the kth entry of $\Theta_1^{(4)}$.

The number of neurons in each layer is an important hyperparameter that needs to be carefully chosen since it controls the model ability to suitably approximate a function. Roughly speaking, the more neurons a DNN model has, the more complicated function can be approximated by the model. A similar argument also holds for the number of hidden layers or data samples. However, having too many parameters or neurons in the model would lead to over-fitting [19]. This is the case when the ML model memorizes its training dataset and yields a prediction based on it, which results in a poor generalized

 $^{^{\}rm I}{\rm Here},\,f_s$ denotes the operation frequency, and the other parameters are defined in Section II.

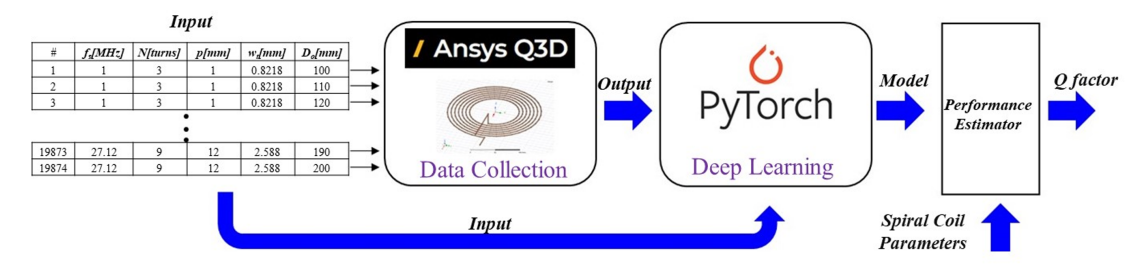


Fig. 3: System architecture, including the data collection, FNN model training, and performance evaluation for the spiral coil design.

performance (i.e., test performance) if a new unseen data (e.g., test data) is different, in a distribution sense, from the training data. To mitigate the over-fitting phenomenon, one usually divides the dataset into three different datasets, namely the training, validation, and test datasets. The training dataset is used to train the ML model, and the validation dataset is used to evaluate the model performance (i.e., validation loss) during the training phase. The test performance is then evaluated based on the test dataset that is unknown to the model during the training phase.

We trained the FNN model by choosing the well-known mean squared error (MSE) loss function defined as,

$$L(f(\mathbf{X}), \mathbf{y}) = \frac{1}{N_D} \sum_{i=1}^{N_D} (f(\mathbf{x}_i; \Theta) - y_i)^2, \tag{9}$$

where: (i) $f(\cdot; \Theta)$ is the FNN model with parameter Θ ; (ii) (\mathbf{X}, \mathbf{y}) is the dataset; (iii) N_D denotes the number of data samples; and (iv) (\mathbf{x}_i, y_i) is the *i*th data sample. In our setting, we used $\mathbf{x}_i = (D_o, f_s, N, p, w_t)$ and $y_i = Q$ for the ith data sample. During the training phase, the parameters Θ 's were optimized by using the stochastic gradient descent algorithm, where we made use of a batch size equal to 160 and a total number of epochs equal to 2,000. Note that the selected number of epochs ensures that our model is not over-fitted to the training dataset. Once the FNN model is trained based on the given dataset (X, y), it readily outputs \hat{Q} , i.e., the estimated value of the Q factor corresponding to the coil design parameters. We trained the FNN model over a spiral coil dataset, as shown in Fig. 3. This block diagram shows the overall procedure of the training phase, including data collection (see Section III-B), FNN model training (see Section III-C), and Q factor evaluation (see Section III-D) of our ML-based spiral coil design.

B. Data Collection

We used the Ansys-Q3D simulator to simulate various spiral coil configurations and, for each of them, we extracted the resulting values of R, L, and C_p (from which the corresponding Q factor can be computed from (6)). The structure of the spiral coil in Ansys-Q3D is shown in Fig. 4 and it is characterized by the geometrical parameters D_o , N, p, and w_t . For each configuration, the spiral coil was wound using the enameled magnet wire, which contains a copper conductor wrapped in 80 μ m polyester. The wire was further extended for the start and finish nodes due to the lead connection. The Ansys-Q3D simulator analyzes the quasi-static electromagnetic field and

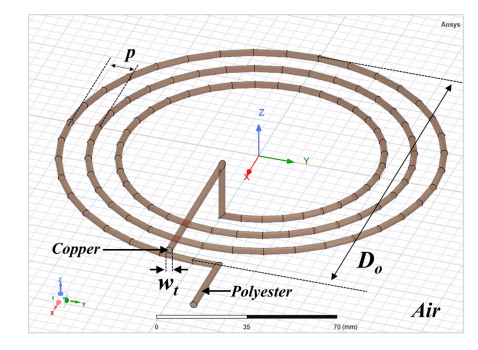


Fig. 4: Spiral coil shape for data collection in the Ansys-Q3D.

extracts the capacitance C, the AC resistance $R_{\rm AC}$ and the AC inductance $L_{\rm AC}$. TABLE I shows the analysis setup for the data collection. The simulation of each design took around $2\sim 5$ minutes using standard desktop computer resources.

TABLE I: Analysis setup of the Ansys-Q3D for data collection.

Setting Parameters	Value		
Solution Selection	C, R_{AC}, L_{AC}		
Maximum # of Passes	10		
Minimum # of Passes	1		
Minimum Converged # of Passes	3		
Percent Error	0.1%		
Percent Refinement Per Pass	0.1%		

The various spiral coil configurations simulated differ in the values of D_o, f_s, N, p , and w_t . In particular, these five input parameters² are chosen to be uniformly distributed in a specific range with a particular resolution. The range of the geometrical parameters D_o, w_t, N, p is determined based on a general-sized drone (i.e., one of the typical battery-powered applications), and the operating frequency f_s is set above MHz for high-power density. The parameters for data collection have an arbitrary range for the verification of the proposed methodology, which may be extended to a wider range depending on the application. TABLE II shows the values of these parameters that we considered in the simulations for the data collection phase. As shown in TABLE II, we simulated a total of $5 \times 7 \times 12 \times 6 \times 11 = 27,720$ configurations, but among these, we only used 19,874 to construct our dataset. In particular, a total of 7,846 configurations were left out since:

²We consider a general circular spiral coil and do not include various operating conditions, such as coupling coefficient and operating temperature.

TABLE II: Parameters used for the data collection phase.

Variables	Values	# of Splits
f_s [MHz]	1, 6.78, 13.56, 20.34, 27.12	5
N [turns]	3, 4, 5, 6, 7, 8, 9	7
p [mm]	1, 2, 3, 4, 5, 6, 7, 8, 9, 10, 11, 12	12
w_t [mm]	0.822, 1.024, 1.290, 1.628, 2.052, 2.588	6
D_o [cm]	10, 11, 12, 13, 14, 15, 16, 17, 18, 19, 20	11

Total: 19,874 (27,720) cases

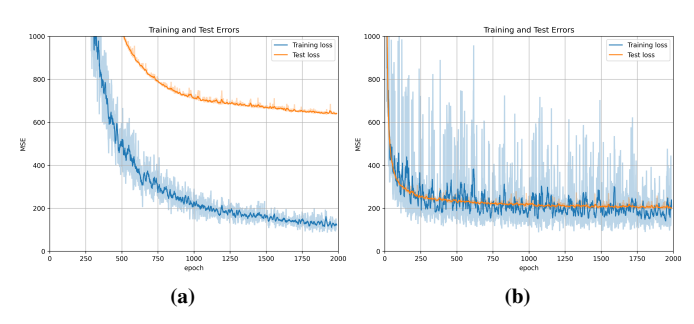


Fig. 5: FNN model training by splitting dataset: (a) 10%/90%; (b) 80%/20%.

(i) 5,645 resulted in a D_i in (1) that was negative; and (ii) 2,201 resulted in a negative Q factor.

C. FNN Training

Our FNN model for estimating the Q factor of the spiral coil was trained using the dataset constructed in Section III-B. As outlined in Section III-A, the designed FNN model contains three hidden layers with 64,128 and 32 neurons in each layer, and the ReLU function was used as the activation function. The inputs were the five parameters D_o, f_s, N, p and w_t , and the output is the Q factor. We applied the stochastic gradient descent algorithm to optimize the model parameters Θ . Specifically, we utilized the ADAM optimizer with learning rate $\gamma=0.001$ to train the model. The MSE, as defined in (9), is the loss function that we used in the training phase.

We randomly split the dataset constructed in Section III-B (19,874 cases) into 8 different training datasets in order to study the effect of the amount of data in our problem. Specifically, these 8 datasets contain from 10% to 80% of data samples, and the remaining data samples are used for test. For instance, the first training dataset contains 10% of the total samples (and the remaining 90% of the total samples are used for test), the second training dataset contains 20% of the total samples (and the remaining 80% of the total samples are used for test), and the eighth training dataset contains 80% of the total samples (and the remaining 20% of the total samples are used for test). We note that a smaller dataset (e.g., 10%dataset) is a subset of a larger dataset (e.g., 20\% dataset). Fig. 5 shows the training and test losses as a function of the training epochs. In Fig. 5, both the training and test losses decrease as the number of training epochs increases. As expected, the test loss in Fig. 5a is greater than the one in Fig. 5b. We note that some training losses in Fig. 5b are greater than the ones in Fig. 5a. This stems from the fact that the smaller dataset in Fig. 5a tends to be easier to fit by the FNN model than the larger dataset. We terminated the training before the model

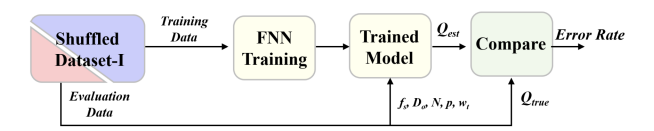


Fig. 6: Block diagram of the evaluation procedures.

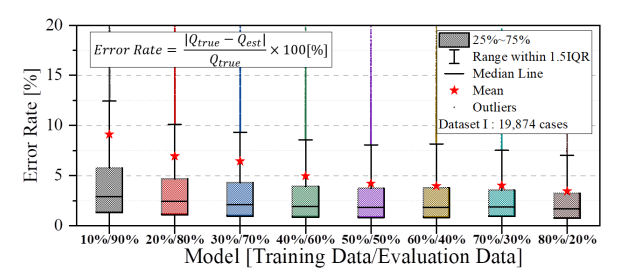


Fig. 7: Error rate distribution of the trained FNN model.

is over-fitted to the training dataset, where we observed that the over-fitting occurs in between 7,000 and 10,000 epochs. Moreover, from Fig. 5, we note that the test loss converges after 1,000 epochs. Based on these considerations, we chose the parameters when the number of epochs is equal to 2,000.

D. Q Factor Evaluation

To verify the effectiveness of our proposed ML-based Q factor estimation, we assessed its accuracy using the evaluation procedure illustrated in Fig. 6. In particular, we performed eight evaluations, i.e., one for each of the eight datasets outlined in Section III-C. Each evaluation utilized the same FNN model and the same number of epochs for training, and the performance was measured in terms of the error rate. In details, for each dataset D_i , $i \in \{1, 2, ..., 8\}$, we used the notation (10i)%/(100%-(10i)%) to denote that (10i)% of the data was used for training and the remaining (100%-(10i)%) of the data was used for test.

From the error rate, we can infer the performance of our proposed ML-based Q factor estimation as a function of the amount of training data. As shown in Fig. 7, the model performance, which is measured in terms of the error rate, improves as the amount of training data increases. In particular, the corresponding average error rate of the 10%/90% model is 9.11% (90.89% accuracy), while the one of the 80%/20% models was 3.45% (96.55% accuracy). This result empirically demonstrates that our ML-based Q factor estimation performs well (the average error rate is below 10%) even when less than 2,000 data samples are used for training.

IV. SPIRAL COIL DESIGN OPTIMIZATION

Our ML-based Q factor estimation proposed in Section III provides the value of the estimated Q factor for a specific spiral coil with fixed values of N, p, D_o, f_s , and w_t . In this section, we take a further practically relevant step in the design of a spiral coil by leveraging our ML-based Q factor estimation proposed in Section III. In particular, we assume that, given the application of interest, only some of the parameters are given, namely D_o and w_t , whereas the

other parameters p, f_s and N can take any value in their ranges, denoted as $\mathcal{S}_p, \mathcal{S}_{f_s}$, and \mathcal{S}_N . Our proposed method then uses the Q factor estimation framework of Section III to select (via an exhaustive searching algorithm) the triplet (p,f_s,N) , such that $p\in\mathcal{S}_p,\,f_s\in\mathcal{S}_{f_s}$ and $N\in\mathcal{S}_N$, that achieves the largest Q factor. In other words, given the values of some spiral coil design parameters, i.e., D_o and w_t , the method estimates the remaining design parameters p,f_s , and N that result in the highest Q factor of the coil. Our proposed method is graphically illustrated in Fig. 8 and it consists of two main building blocks, namely the trained ML-based Q factor estimator of Section III and a searching algorithm. Moreover, a high-level view of our method in terms of a pseudo-code is given in Algorithm 1.

Algorithm 1: ML-based spiral coil design method

```
\begin{aligned} \textbf{Data:} \ & D_o, w_t, \mathcal{S}_p, \mathcal{S}_N, \mathcal{S}_{f_s} \\ \textbf{Result:} \ & \hat{p}, \hat{f}_s, \hat{N}, Q_{\max} \ \text{and} \ \mathcal{I} \\ \text{Initiate} \ & Q_{\max} = 0, \ \hat{p} = 0, \ \hat{f}_s = 0, \ \text{and} \ \hat{N} = 0 \\ \textbf{for} \ & p \in \mathcal{S}_p, f_s \in \mathcal{S}_{f_s} \ \textit{and} \ N \in \mathcal{S}_N \ \textbf{do} \\ & Q \leftarrow \text{FNN}(D_o, f_s, w_t, p, N) \\ \text{Stack} \ & (p, f_s, N, Q) \ \text{in} \ \mathcal{I} \\ & \textbf{if} \ & Q \geq Q_{\max} \ \textbf{then} \\ & | \ & \text{Update} \ & Q_{\max} \leftarrow Q \\ & | \ & \text{Update} \ & \hat{p} \leftarrow p, \ \hat{f}_s \leftarrow f_s \ \text{and} \ & \hat{N} \leftarrow N \\ & \textbf{end} \end{aligned}
```

As shown in Algorithm 1, the method requires a fixed pair (i.e., D_o and w_t) and three sets of feasible values for p, f_s and N (i.e., S_p, S_{f_s} , and S_N). The method provides the best (i.e., having the largest Q factor) values for the design parameters p, f_s and N (denoted as \hat{p}, f_s and N) among every triplet of elements in S_p, S_{f_s} and S_N . In particular, the method first initiates the variables $Q_{\text{max}} = 0, \hat{p} = 0, \hat{f}_s = 0,$ and $\hat{N} = 0$ that represent the maximum value of the Q factor, the best pitch size, the best frequency, and the best number of turns, respectively. In order to find the best parameters \hat{p}, f_s and N among all of the elements in $\mathcal{S}_p, \mathcal{S}_{f_s}$ and S_N , the method iteratively runs the Q factor estimator designed in Section III for every possible triplet (p, f_s, N) (i.e., exhaustive search over S_p , S_f and S_N). At every iteration, the Q factor estimator evaluates the quality of the coil according to $(D_o, f_j, w_t, p_i, N_k)$ for all (i, j, k), where³ $p_i \in \mathcal{S}_p, i \in \{1, \dots, |\mathcal{S}_p|\}, f_j \in \mathcal{S}_{f_s}, j \in \{1, \dots, |\mathcal{S}_{f_s}|\}$ and $N_k \in \mathcal{S}_N, k \in \{1, \dots, |\mathcal{S}_N|\}$. The estimated Q factor is then compared with $Q_{\rm max}$, and if it is larger than $Q_{\rm max}$, then $(\hat{p}, f_s, \hat{N}, Q_{\text{max}})$ is updated such that $\hat{p} = p_i, \ \hat{f}_s = f_j, \ \hat{N} = f_j$ N_k , and $Q_{\text{max}} = Q$. Moreover, each tuple (p_i, f_i, N_k, Q) from the Q factor estimator is always stored in \mathcal{I} so that it can be leveraged later. After running all of the iterations in the searching algorithm, the tuple $(\hat{p}, \hat{f}_s, \hat{N}, Q_{\text{max}})$ provides the best parameters and the corresponding estimated Q factor, which is the maximum over all of the estimated Q factors, resulting from all $p \in \mathcal{S}_p, f_s \in \mathcal{S}_{f_s}$ and $N \in \mathcal{S}_N$.

Beyond estimating one triplet of optimal parameters for the spiral coil (i.e., \hat{p} , \hat{f}_s and \hat{N}), our method also provides a top-k% region of p, f_s and N for each fixed pair (D_o, w_t) . Specifically, this region contains all the triplets $(p, f_s, N) \in \mathcal{S}_p \times \mathcal{S}_{f_s} \times \mathcal{S}_N$ in \mathcal{I} that produce a Q factor with an error rate smaller than k% from the highest Q factor. In other words, we say that a design belongs to the top-k% region if its Q factor is at least (100-k)% of the highest Q factor among the designs with the same D_o and w_t . We refer to this procedure as top-k% filtering as shown in Fig. 8.

A. Numerical Evaluation

Here, we numerically assess the effectiveness of our proposed spiral coil design. Towards this end, we adopt the IoU metric, which, given two regions, is defined as the ratio between the volume of their overlap and the volume of their union [13]. Specifically, the two regions that we consider are the top-k% region provided by our proposed method, and the true⁴ top-k% region. In order to build these two regions (and hence, evaluate the IoU factor) we made use of an interpolation technique [23] over the discrete triplets (p, f_s, N) . Fig. 9 provides a graphical illustration of the used evaluation method.

As shown in Fig. 9, the IoU increases with the volume of the overlap region, and we wish that our method has a large IoU, as close as possible to one. This, in fact, would imply that our proposed method provides a design that belongs to the true top-k% region with high probability.

The evaluation results, shown in Fig. 10, consider k=10 and they represent the IoUs averaged over 66 pairs⁵ of (D_o, w_t) . From Fig. 10, we observe that the maximum IoU is of 69.7%, which is indeed moderately a high score in the 3-dimensional case. Moreover, our method performs well (i.e., IoU is more than 56%) even when the amount of training data is less than 1,000 samples (i.e., around 5% of the total 19,874 samples). We also note that the computation time to obtain the best design (i.e., top-k% region) over 1,000 designs with our method was around a second (i.e., 1.65 seconds), whereas Ansys-Q3D took $2 \sim 5$ minutes to test a single design, leading to requiring roughly at least 2,000 minutes to run a searching algorithm over the same 1,000 designs.

V. EXPERIMENTAL RESULTS

In this section, we assess and verify the performance of the proposed ML-based spiral coil design of Section IV through experiments with the actual fabrication of some samples of the spiral coil. For precise fabrication, the coils were custom-made using winding bobbins and magnetic copper wire. The winding bobbins were designed with a computer-aided design (CAD) tool and fabricated using a 3D printer with polylactide (PLA) plastic materials without any additional magnetic materials. In order to connect with the measurement equipment, an additional PCB, an SMA connector, and a variable capacitor for resonance were attached to the ends of the coil nodes.

³For a set A, the notation |A| indicates the cardinality of A.

 $^{^4}$ The true best design is the spiral coil design with the highest Q factor in the dataset built in Section III using the Ansys-Q3D simulator.

⁵In Fig. 10, we considered $D_o \in \{100, 110, ..., 190, 200\}$ and $w_t \in \{0.8128, 1.0236, 1.2903, 1.6281, 2.0523, 2.5883\}$.

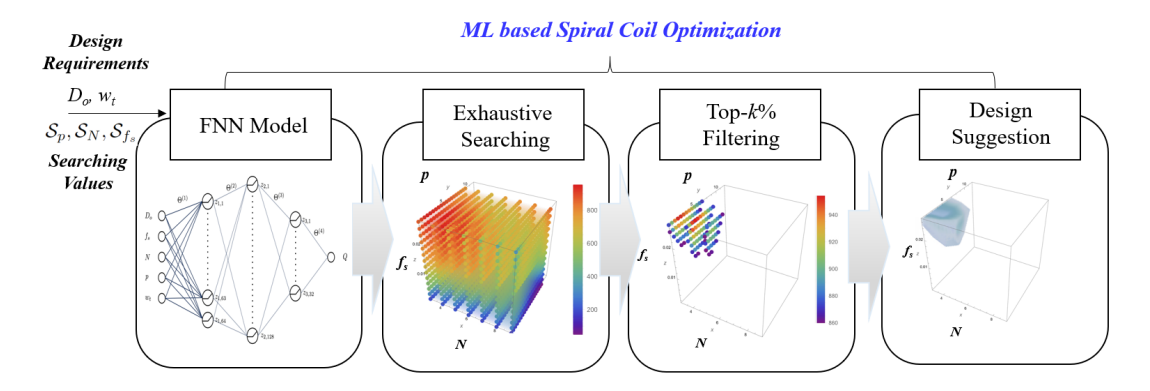


Fig. 8: Detailed configuration of the ML-based coil optimization.

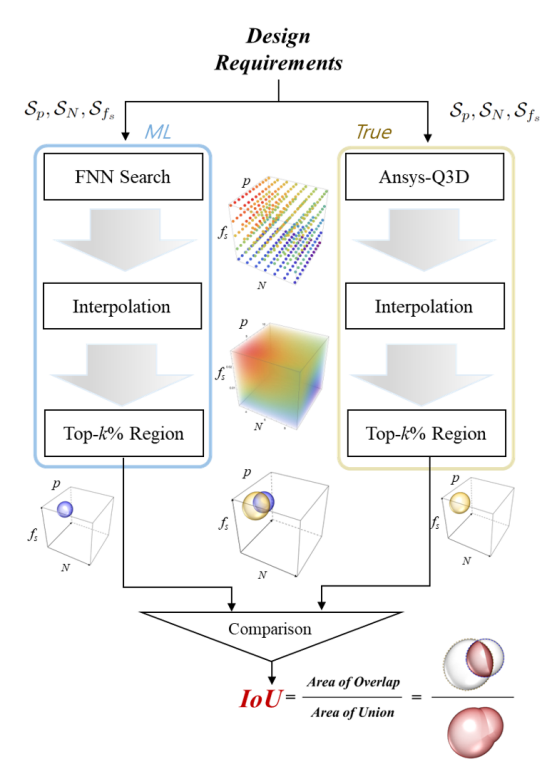


Fig. 9: Evaluation method between the estimated and the true top-k% regions using the IoU.

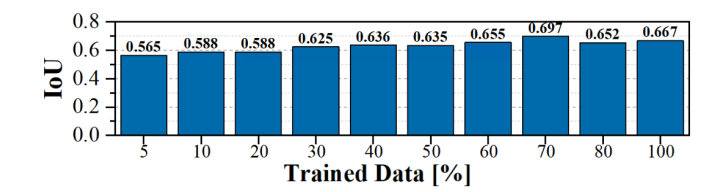


Fig. 10: Average IoU versus amount of training data when k=10. The FNN model was trained over 1,000 epochs.

As an application environment to test the proposed design method, we considered $D_o=100$ mm and $w_t=2.588$ mm. Based on these values, our ML-based coil design method of Section IV outputted the top-10% region as a function of p, f_s , N, as shown in Fig. 11a. We further divided our experiment into two sub-experiments, namely Experiment-A, in which we fixed $f_s=20.34$ MHz, and Experiment-B, in which we fixed p=3 mm. The top 10% region for Experiment-A (respectively, Experiment-B) was provided as shown in Fig. 11b (respectively, Fig. 11c).

Based on these top 10% regions, for both Experiment-A and Experiment-B, we fabricated seven spiral coils (see the red dots and stars in Fig. 11b and Fig. 11c). In particular, for Experiment-A, we considered values of N and p as shown in Fig. 12a, and for Experiment-B, we considered values of N and f_s as shown in Fig. 12b.

For each experiment design, we measured the resistance R_{eq} and reactance X_{eq} (from which we can compute the Q factor using (5)) using the Vector Network Analyzer (E5061B from Keysight Technologies). In particular, the resistance R_{eq} was measured in a series resonance condition with an additional variable capacitor in order to reduce the measurement error due to the ratio between the resistance and the reactance [14], [17]. From Fig. 11b, we observe that the pair p = 3 mm and N = 4 (i.e., A2 in Fig. 12) achieves the largest Qfactor (star point in Fig. 11b). Similarly, from Fig. 11c, we observe that the pair $f_s = 27.12$ MHz and N = 3 (i.e., B1 in Fig. 12b) achieves the largest Q factor (star point in Fig. 11c). Fig. 11b and Fig. 11c verify that the best spiral coil designs indeed fall within the top-10% regions provided by our proposed ML-based coil design method, hence showcasing its effectiveness. Our experiments showcased a few discrepancies between the Q factor values obtained via Ansys-Q3D and those measured in the fabricated coils. We suspect that these are due to several reasons, such as: (i) the presence of an additional series capacitor C_s to create the series resonance; (ii) an additional resistance due to soldering or a contact resistance in the measurement phase; and (iii) a measurement error of the equivalent resistance R_{eq} due to factors such as calibration accuracy, noise, and other sources of uncertainty.

For further verification, the performance of the AC-to-AC WPT system was measured using coils A1, A2, A3, and A4

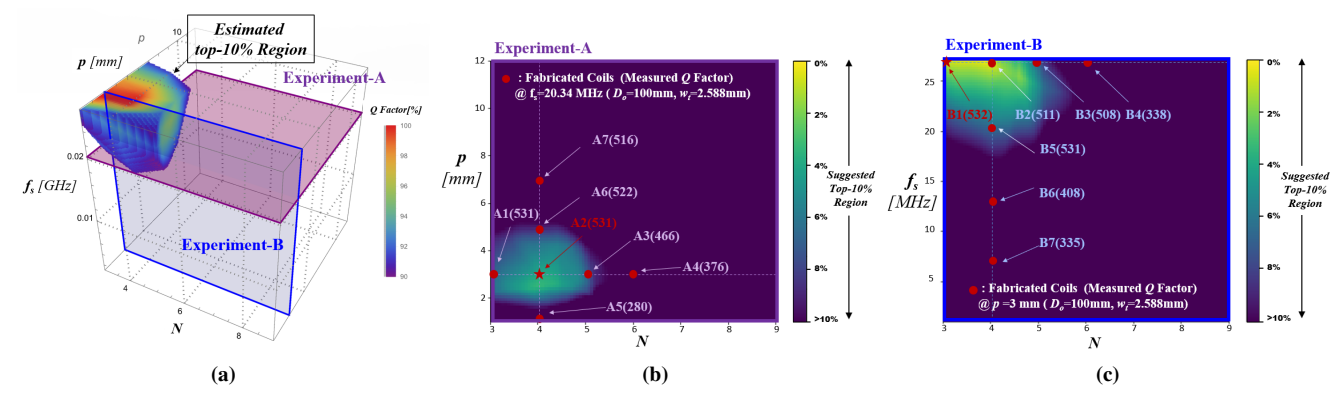


Fig. 11: Verification of the proposed coil design method. (a) Top-10% region. (b) Experiment-A: Estimated top-10% region, and measured results of the fabricated coils; $D_o = 100$ mm, $f_s = 20.34$ MHz, $w_t = 2.588$ mm. (c) Experiment-B: Estimated top-10% region, and measured results of the fabricated coils; $D_o = 100$ mm, p = 3 mm, $w_t = 2.588$ mm.

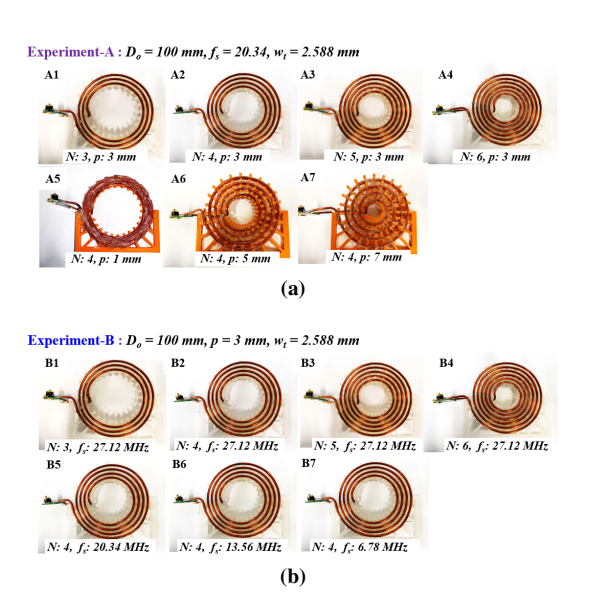


Fig. 12: Fabricated coils for demonstration of the ML-based coil optimization: (a) Experiment-A; (b) Experiment-B.

from Experiment-A, along with B2, B5, B6, and B7 from Experiment-B. In this AC-to-AC WPT system, we fabricated two identical coils for each case, designating one as the transmitter coil Tx and the other as the receiver coil Rx. Additional capacitors were connected to these coils to create a seriesseries compensation network within the WPT system. The value of C_s was calculated based on the measured inductance L_{eq} and on the numerical equations for series resonance [24]. The specific values are presented in TABLE III.

Before testing the WPT system, we measured the input impedance and the coupling coefficient using a Vector Network Analyzer (E5061B from Keysight Technologies). These parameters were measured at the transmitter side by changing the distance between the Tx coil and the Rx coil under well-aligned conditions. We determined the coupling coefficient between the two series compensated coils as follows,

$$k = \frac{2(f_h - f_l)}{f_h + f_l},\tag{10}$$

TABLE III: Additional capacitors C_s for the series-series compensation network [24].

Coil	f_s [MHz]	L_{eq} [μ H]	$C_s [pF]$
A1	20.34	1.39	44
A2(=B5)	20.34	2.08	29.3
A3	20.34	2.77	22.1
A4	20.34	3.24	18.9
B2	27.12	2.56	13.5
В6	13.56	1.83	753
B7	6.78	1.71	322

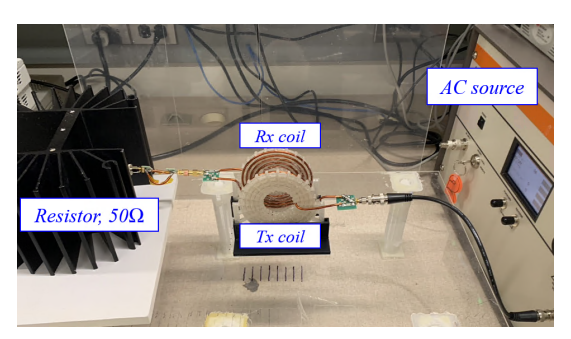
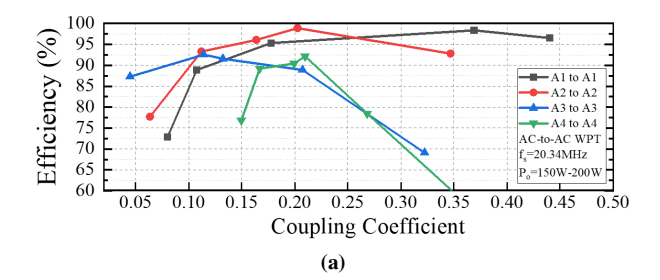


Fig. 13: Experimental setup of the AC-to-AC WPT system using the designed coils.

where f_h and f_l are the higher and lower split frequencies of the two coupled resonators, respectively.

The experimental setup for the AC-to-AC WPT system is depicted in Fig. 13. The transmitter coil was connected to the RF power amplifier (AR RF/Microwave Instrumentation, 500A250C), and a function generator was used to generate high-frequency reference signals for RF amplifier operation. On the receiver side, a 500 W and 50 Ω RF resistor was connected with the Rx coil. The conversion efficiency was calculated by measuring the input power on the RF amplifier display panel, and the output power was assessed using tuned voltage/current probes connected to an oscilloscope (Keysight Tech., MSOX3034T). The conversion efficiency of the tested AC-to-AC system is illustrated in Fig. 14. Among coils A1,

A2, A3, and A4 in Experiment-A, coil A2 exhibited the highest efficiency compared to the other coils. Similarly, among coils B2, B5, B6, and B7 in Experiment-B, coil B5 outperformed the other coils in terms of conversion efficiency. As suggested by the top-k% regions in Fig. 11b and Fig. 11c, the efficiencies of coils A1 and A2 (also, B2 and B5) were higher than the other two. These results indicate that our ML-based optimization method provides a reasonable design solution, leading to the highest conversion efficiency.



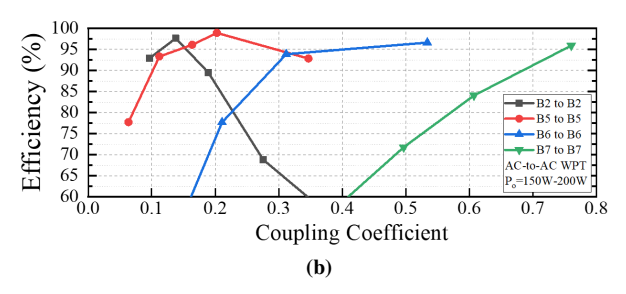


Fig. 14: Measured conversion efficiency of the AC-to-AC WPT system depending on the coupling coefficient (a) Experiment-A; (b) Experiment-B.

One of the appealing features of our proposed ML-based spiral coil design method is its computation time in providing suitable guidelines for the design and fabrication of a coil. As shown in Fig. 15, the proposed method takes around 1.65 seconds to derive the top-k% region for a fixed pair (D_o, w_t) and 1,000 triplets of (p, f_s, N) . In contrast, simulation tools such as Ansys-Q3D and Ansys-HFSS take around 2 minutes (Ansys-Q3D) and 16 minutes (Ansys-HFSS) for each triplet (p, f_s, N) . This means that it takes approximately 33 hours (Ansys-Q3D) and 267 hours (Ansys-HFSS) to search over 1,000 triplets (p, f_s, N) for optimization. Therefore, our proposed spiral coil design method offers significant time savings for the design and optimization of a spiral coil.

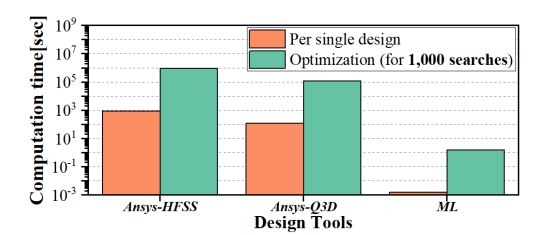


Fig. 15: Comparison of the computation time for the spiral coil design.

In summary, our ML-based coil design method provides several advantages over traditional approaches, as also illustrated in TABLE IV. The proposed ML-based design method allows us to design coils, with different sizes and at different frequencies, having a large Q factor without any complicated analysis or long simulations. Specifically, our design method leverages the collected dataset and provides a design solution with reduced computational time and high accuracy. While an analytical method, which computes the expressions in (2)-(4), can optimize a design quickly, it relies on simplified equations, which are often inaccurate and must be redefined depending on the environment of interest. Differently, our FNN method utilizes a data-based trained model for optimization (instead of analytic equations). Because of this, our FNN method is adaptable to design changes; it also offers a fast optimization and it provides a high accuracy.

Also, finite element analysis (FEA) simulators extract accurate results and are adaptable to various designs, provided that a precise 3D CAD model is available. However, they may require a long time to extract accurate results, as we also demonstrated in Fig. 15. This would lead to a reduced productivity in industrial applications. Our proposed method promises accuracy and effective computational times, as long as the training dataset is accurate. Even though we have only utilized five design parameters, along with the evaluation metric (Q factor), it is possible to incorporate additional parameters or any other evaluation metric or index to train and optimize the designs. Particularly, our optimization method employs a searching algorithm to effectively output the topk% optimal designs without requiring the calculation of the lumped elements or of the impedance. The proposed method provides an intuitive and flexible approach to coil optimization. This suggests that our design method has the potential to be employed by 'data-rich industries' that possess a large number of diverse datasets.

VI. CONCLUSION

This paper presented a spiral coil design for WPT systems using an ML-based optimization method. The proposed method first accurately estimated the Q factor using ML, which was then leveraged to obtain the top-k region for selecting the best design of the coil in a specific environment. The method was successfully evaluated in several test cases, showing an up to 70% overlap between the estimated and the true top-k% regions. In addition, the performance of the proposed optimization method was verified through the fabrication and testing of actual coils, with the optimal p, N and f_s values found to be in agreement with those provided by the ML-based optimization method. Both numerical and experimental results confirmed the effectiveness (both in terms of accuracy and computation time) of the proposed method as a design tool for spiral coils in WPT systems.

REFERENCES

- S. Y. R. Hui, W. Zhong, and C. K. Lee, "A critical review of recent progress in mid-range wireless power transfer," *IEEE Transactions on Power Electronics*, vol. 29, no. 9, pp. 4500–4511, 2014.
- [2] S. Aldhaher, P. D. Mitcheson, J. M. Arteaga, G. Kkelis, and D. C. Yates, "Light-weight wireless power transfer for mid-air charging of drones," in 2017 11th European Conference on Antennas and Propagation (EUCAP), 2017, pp. 336–340.
- [3] R. Ito, Y. Sawahara, T. Ishizaki, and I. Awai, "Construction of a secure wireless power transfer system for robot fish," in 2015 IEEE Wireless Power Transfer Conference (WPTC), 2015, pp. 1–4.

Methods	Preparation	Optimization time	Accuracy	Design Flexibility	Industrial Applications
Analytical Method [16], [25]	R, L, C_p, Q Formulas	Fast	Low	Bad	Bad
FEA Simulation [11], [26], [27]	Simulators, CAD design	Slow	Very High	Medium	Medium
Proposed Method	Dataset and Trained Model	Fast	High	Good	Good

TABLE IV: Comparison of design methods for the coil optimization.

- [4] A. Karalis, J. Joannopoulos, and M. Soljačić, "Efficient wireless non-radiative mid-range energy transfer," *Annals of Physics*, vol. 323, no. 1, pp. 34 48, 2008, january Special Issue 2008. [Online]. Available: http://www.sciencedirect.com/science/article/pii/S0003491607000619
- [5] S. Li and C. C. Mi, "Wireless power transfer for electric vehicle applications," *IEEE Journal of Emerging and Selected Topics in Power Electronics*, vol. 3, no. 1, pp. 4–17, 2015.
- [6] G. Grandi, M. Kazimierczuk, A. Massarini, and U. Reggiani, "Stray capacitances of single-layer air-core inductors for high-frequency applications," in IAS '96. Conference Record of the 1996 IEEE Industry Applications Conference Thirty-First IAS Annual Meeting, vol. 3, 1996, pp. 1384–1388 vol.3.
- [7] Z. Jiang, P. Excell, and Z. Hejazi, "Calculation of distributed capacitances of spiral resonators," *IEEE Transactions on Microwave Theory and Techniques*, vol. 45, no. 1, pp. 139–142, 1997.
- [8] I. Lope, C. Carretero, and J. Acero, "First self-resonant frequency of power inductors based on approximated corrected stray capacitances," *IET Power Electronics*, vol. 14, no. 2, pp. 257–267, 2021. [Online]. Available: https://ietresearch.onlinelibrary.wiley.com/doi/abs/ 10.1049/pel2.12030
- [9] V. Shevchenko, O. Husev, R. Strzelecki, B. Pakhaliuk, N. Poliakov, and N. Strzelecka, "Compensation topologies in ipt systems: Standards, requirements, classification, analysis, comparison and application," *IEEE Access*, vol. 7, pp. 120559–120580, 2019.
- [10] C.-S. Wang, G. Covic, and O. Stielau, "Power transfer capability and bifurcation phenomena of loosely coupled inductive power transfer systems," *IEEE Transactions on Industrial Electronics*, vol. 51, no. 1, pp. 148–157, 2004.
- [11] M. Kim, S. Park, and H.-K. Jung, "An advanced numerical technique for a quasi-static electromagnetic field simulation based on the finite-difference time-domain method," *Journal of Computational Physics*, vol. 373, pp. 917–923, 2018. [Online]. Available: https://www.sciencedirect.com/science/article/pii/S0021999118304935
- [12] Q. Chen and A. Konrad, "A review of finite element open boundary techniques for static and quasi-static electromagnetic field problems," *IEEE Transactions on Magnetics*, vol. 33, no. 1, pp. 663–676, 1997.
- [13] H. Rezatofighi, N. Tsoi, J. Gwak, A. Sadeghian, I. Reid, and S. Savarese, "Generalized intersection over union: A metric and a loss for bounding box regression," in 2019 IEEE/CVF Conference on Computer Vision and Pattern Recognition (CVPR), 2019, pp. 658–666.
- [14] M. Kim, M. Jeong, M. Cardone, and J. Choi, "Characterization of the quality factor in spiral coil designs for high-frequency wireless power transfer systems using machine learning," in 2022 IEEE 23rd Workshop on Control and Modeling for Power Electronics (COMPEL), 2022, pp. 1–8
- [15] M. Kim, M. Jeong, M. Cardone, and J. Choi, "Optimization of spiral coil design for wpt systems using machine learning," in 2023 IEEE Applied Power Electronics Conference and Exposition (APEC), 2023.
- [16] B. H. Waters, B. J. Mahoney, G. Lee, and J. R. Smith, "Optimal coil size ratios for wireless power transfer applications," in 2014 IEEE International Symposium on Circuits and Systems (ISCAS), 2014, pp. 2045–2048.
- [17] J. Lawson, D. C. Yates, and P. D. Mitcheson, "High q coil measurement for inductive power transfer," *IEEE Transactions on Microwave Theory and Techniques*, vol. 67, no. 5, pp. 1962–1973, 2019.
- [18] S. Li and C. C. Mi, "Wireless power transfer for electric vehicle applications," *IEEE Journal of Emerging and Selected Topics in Power Electronics*, vol. 3, no. 1, pp. 4–17, 2015.
- [19] C. M. Bishop and N. M. Nasrabadi, Pattern recognition and machine learning. Springer, 2006, vol. 4, no. 4.
- [20] I. Goodfellow, Y. Bengio, and A. Courville, *Deep learning*. MIT press, 2016.
- [21] J. Park and I. W. Sandberg, "Universal approximation using radial-basisfunction networks," *Neural Computation*, vol. 3, no. 2, pp. 246–257, 1991

- [22] B. Hanin, "Universal function approximation by deep neural nets with bounded width and relu activations," *Mathematics*, vol. 7, no. 10, p. 992, 2019.
- [23] G. Wahba, Spline models for observational data. SIAM, 1990.
- [24] M. Kim and J. Choi, "Design of self-resonant spiral coils for mid-range, high-frequency wireless power transfer systems," in 2022 Wireless Power Week (WPW), 2022, pp. 33–38.
- [25] Z. Luo and X. Wei, "Analysis of square and circular planar spiral coils in wireless power transfer system for electric vehicles," *IEEE Transactions* on *Industrial Electronics*, vol. 65, no. 1, pp. 331–341, 2018.
- [26] T. Hou, J. Xu, W. S. Elkhuizen, C. C. L. Wang, J. Jiang, J. M. P. Geraedts, and Y. Song, "Design of 3d wireless power transfer system based on 3d printed electronics," *IEEE Access*, vol. 7, pp. 94793–94805, 2019.
- [27] R. Qin, J. Li, and D. Costinett, "A 6.6-kw high-frequency wireless power transfer system for electric vehicle charging using multilayer nonuniform self-resonant coil at mhz," *IEEE Transactions on Power Electronics*, vol. 37, no. 4, pp. 4842–4856, 2022.



Minki Kim received his BS degree in electrical engineering from Kyungpook National University (KNU), Daegu, Rep. of Korea, in 2008, and his MS degree in electrical engineering from Seoul National University (SNU), Rep. of Korea, in 2010. From 2010 to 2019, he has worked at the Electronics and Telecommunication Research Institute (ETRI), Daejeon, Rep. of Korea as a senior research engineer. He is studying as a Ph.D. student at the University of Minnesota from 2019. His research interests include wireless power transfer systems,

wide bandgap power devices, and power control systems.



Minoh Jeong received a B.Sc. degree in electronic engineering from Inha University, South Korea, in 2017, and a M.Sc. degree in electrical and computer engineering from Ajou University, South Korea, in 2019. He is currently pursuing a Ph.D. degree with the Electrical and Computer Engineering Department, the University of Minnesota. His research interests include statistical signal processing, differential privacy, machine learning, coding theory, and information theory.



Martina Cardone (Senior Member, IEEE) received the Ph.D. degree in electronics and communications from Télécom ParisTech (with work done with Eurecom, Sophia Antipolis, France) in 2015. She is currently a McKnight Land-Grant Assistant Professor with the Electrical and Computer Engineering Department, University of Minnesota (UMN). From November 2017 to January 2018, she was a Post-Doctoral Associate with the Electrical and Computer Engineering Department, UMN. From July 2015 to August 2017, she was a Post-Doctoral Research

Fellow with the Electrical and Computer Engineering Department, Henry Samueli School, UCLA. Her main research interests include estimation theory, network information theory, network coding, and wireless networks, with a special focus on their capacity, security, and privacy aspects. She was a recipient of the 2022 McKnight Land-Grant Professorship, the NSF CAREER Award in 2021, the NSF CRII Award in 2019, the Second Prize in the Outstanding Ph.D. Award, Télécom ParisTech, Paris, France, and the Qualcomm Innovation Fellowship in 2014.



Jungwon Choi (S'13-M'19) received the B.Eng. degree in electrical engineering from Korea University, Seoul, South Korea, in 2009, the M.S.E. degree in electrical engineering from the University of Michigan, Ann Arbor, MI, USA, in 2013, and the Ph.D. degree in electrical engineering from Stanford University, Stanford, CA, USA, in 2019. From 2019 to 2023, she was an Assistant Professor with the University of Minnesota, Twin Cities, Minneapolis, MN, USA. In 2023, she joined the University of Washington, Seattle, WA, USA, as an Assistant

Professor with the Department of Electrical and Computer Engineering. Her research interests include high-frequency high-power converters with wide-bandgap devices for wireless power transfer applications, the design of passive components in wireless power transfer, and power converters for renewable energy systems.